

CHAPTER 1

Appendix

1.1 Jordan normal form of infinite matrix sum

In this section, we show that for a matrix A with spectral radius less than one, the eigenvalues of $B = \sum_{k=1}^{\infty} A^k$ are exactly $\frac{\lambda_i}{1-\lambda_i}$ for $\lambda_i \in \sigma(A)$. It is easy to show that if (λ, v) is an eigenpair of B , then $\left(\frac{\lambda}{1-\lambda}, v\right)$ is an eigenpair of B . However, it is not immediately clear if these are all the eigenpairs of B and hence the eigenvalues. Namely, if the algebraic and geometric multiplicities of the eigenvalues are not the same. To show this, let J be the Jordan normal form of A such that A is similar to J by some invertible matrix P . In particular, the Jordan normal form consists of Jordan blocks J_i such that

$$J = \begin{bmatrix} J_1 & & & \\ & J_2 & & \\ & & \ddots & \\ & & & J_p \end{bmatrix}$$

Hence, B can be written as

$$B = \sum_{k=1}^{\infty} A^k = \sum_{k=1}^{\infty} P^{-1} J^k P = P^{-1} \sum_{k=1}^{\infty} J^k P$$

Note that J^k is given by

$$J^k = \begin{bmatrix} J_1^k & & & \\ & J_2^k & & \\ & & \ddots & \\ & & & J_p^k \end{bmatrix}$$

Focusing on a single Jordan block J_i given by

$$J_i = \begin{bmatrix} \lambda_i & 1 & & \\ & \lambda_i & 1 & \\ & & \ddots & \\ & & & \lambda_i \end{bmatrix},$$

we see that $J_i^k = \lambda_i^k I + T$ where T is a strictly upper-triangular matrix. From this, we see that $\sum_{k=1}^{\infty} J_i^k = \frac{\lambda_i}{1-\lambda_i} I + T'$ where T' is another strictly upper-triangular matrix. Thus, $\sum_{k=1}^{\infty} J_i^k$ has $\frac{\lambda_i}{1-\lambda_i}$ as diagonal elements, hence there exists some invertible matrix P_i such that $\sum_{k=1}^{\infty} J_i^k = (P_i)^{-1} J'_i P_i$ where J'_i is a Jordan normal form (with $\frac{\lambda_i}{1-\lambda_i}$ as diagonal elements) of $\sum_{k=1}^{\infty} J_i^k$. Combining the above, we have that

$$\begin{aligned} \sum_{k=1}^{\infty} J^k &= \begin{bmatrix} \sum_{k=1}^{\infty} J_1^k & & & \\ & \sum_{k=1}^{\infty} J_2^k & & \\ & & \ddots & \\ & & & \sum_{k=1}^{\infty} J_p^k \end{bmatrix} \\ &= \begin{bmatrix} P_1^{-1} J'_1 P_1 & & & \\ & P_2^{-1} J'_2 P_2 & & \\ & & \ddots & \\ & & & P_p^{-1} J'_p P_p \end{bmatrix} \\ &= \begin{bmatrix} P_1 & & & \\ & P_2 & & \\ & & \ddots & \\ & & & P_p \end{bmatrix}^{-1} \begin{bmatrix} J'_1 & & & \\ & J'_2 & & \\ & & \ddots & \\ & & & J'_p \end{bmatrix} \begin{bmatrix} P_1 & & & \\ & P_2 & & \\ & & \ddots & \\ & & & P_p \end{bmatrix} \end{aligned}$$

Let P' be the above block diagonal matrix, consisting of P_i 's and J' be the block diagonal matrix consisting of J'_i 's and hence also a Jordan normal form. Then, we can finally write B as

$$B = (P' P)^{-1} J' P' P$$

In particular, B is similar to the Jordan normal form J' with diagonal elements $\frac{\lambda_i}{1-\lambda_i}$. In particular, the spectrum of B is exactly the elements of the spectrum of A mapped by $\lambda \mapsto \frac{\lambda}{1-\lambda}$.

1.2 Pharmaceutical duration and level changes plots

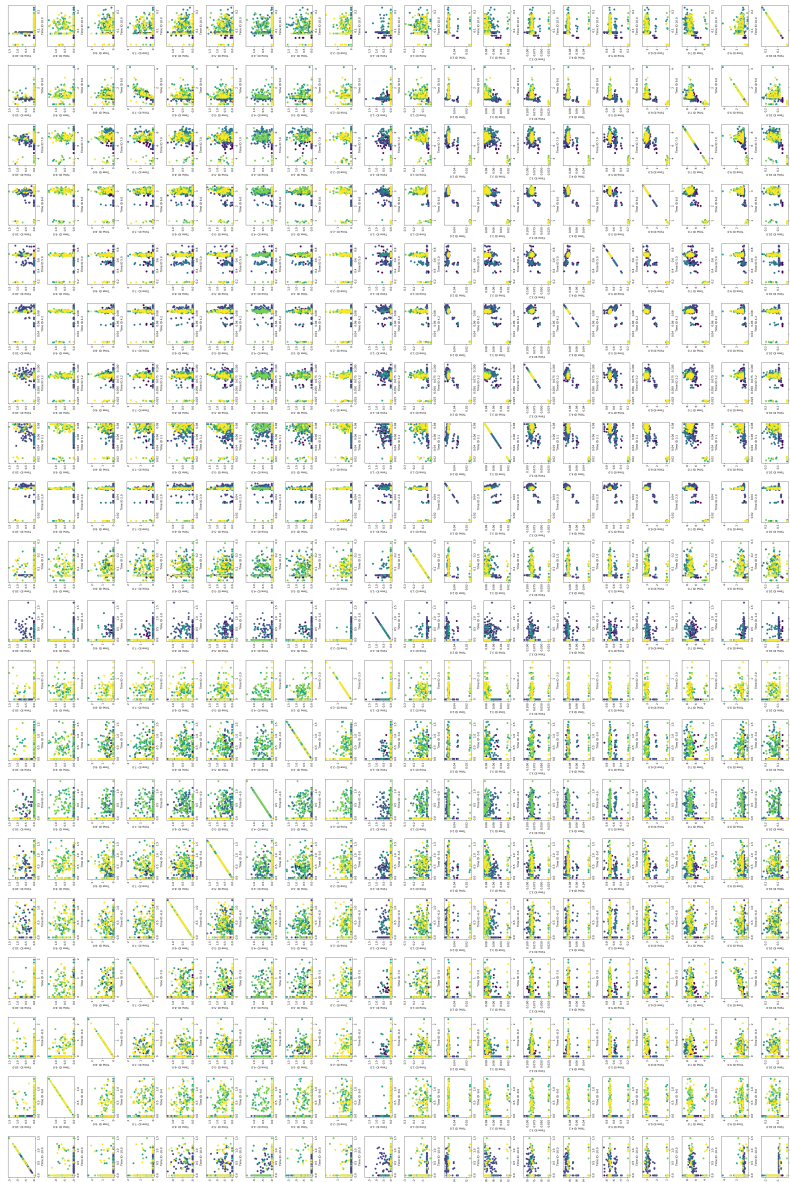


Figure 1.1: Durations and delays vs durations and delays. Some combinations of variables show a tendency, although a causal structure can not be inferred from this alone.

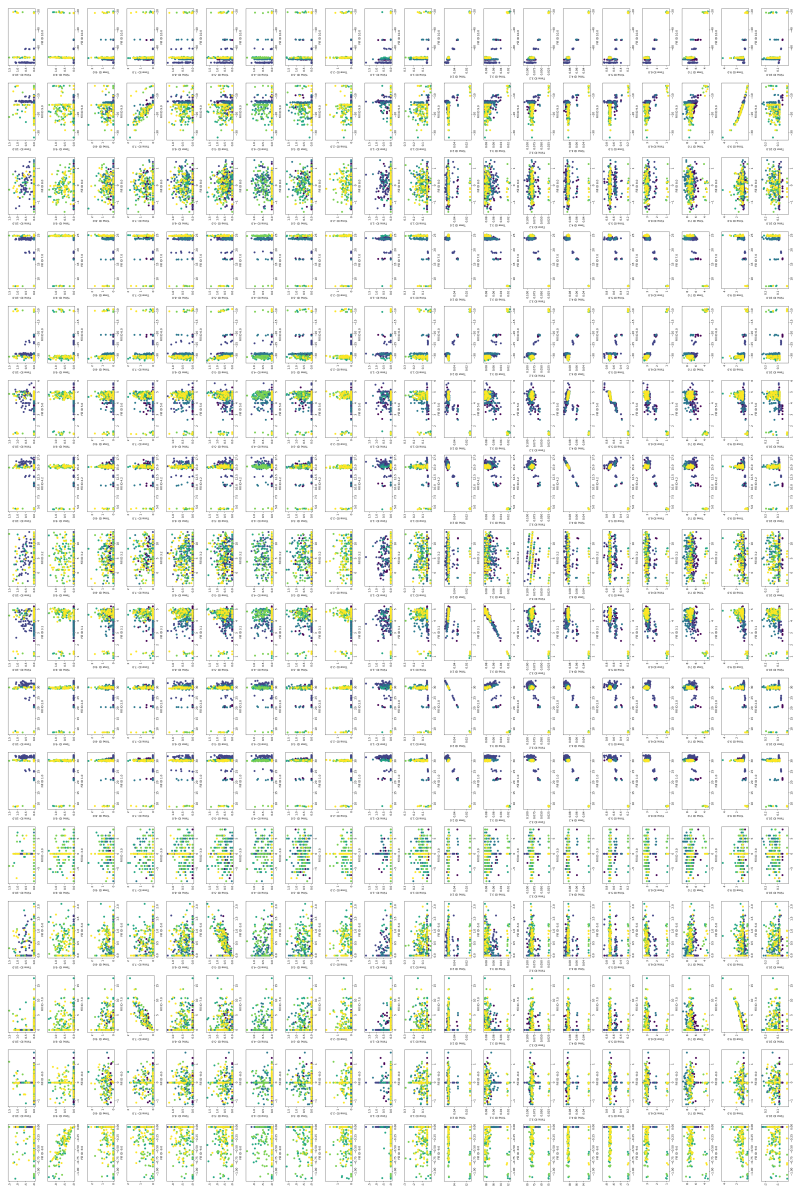


Figure 1.2: Changes in levels vs durations and delays.

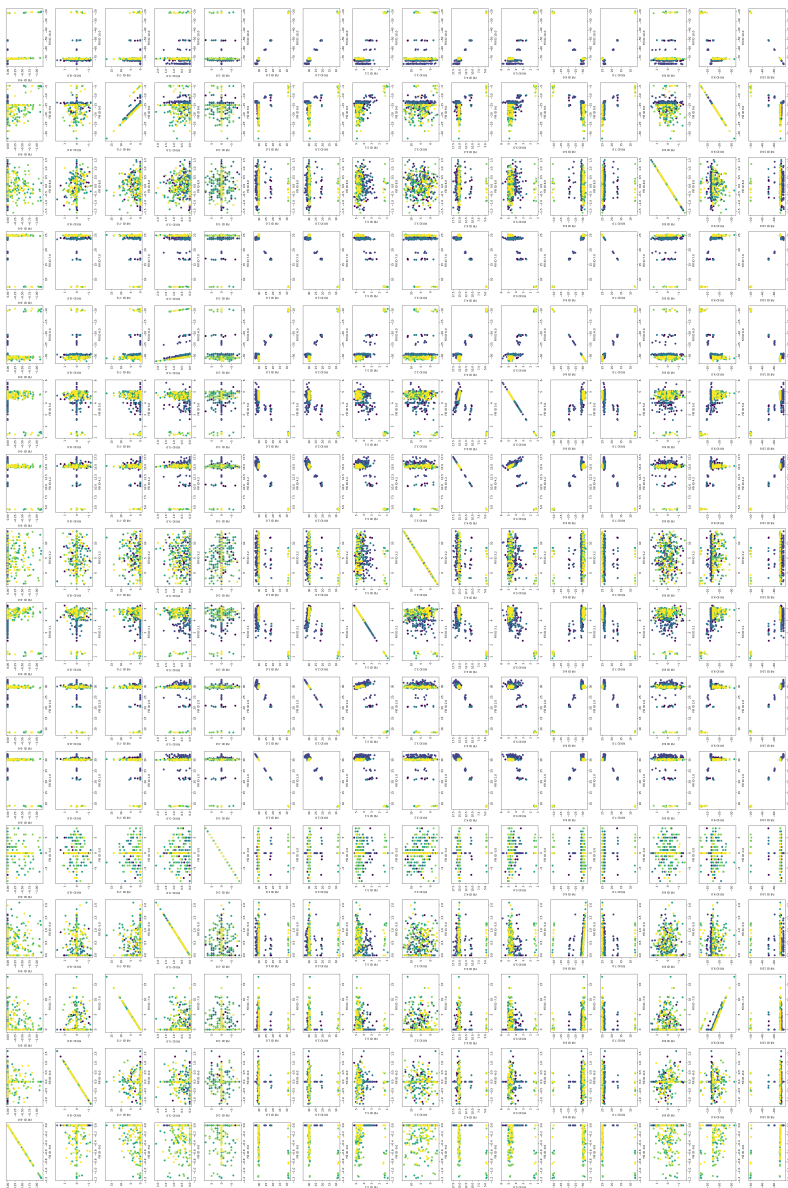


Figure 1.3: Changes in levels vs changes in levels.

1.3 Cleaning operations plots

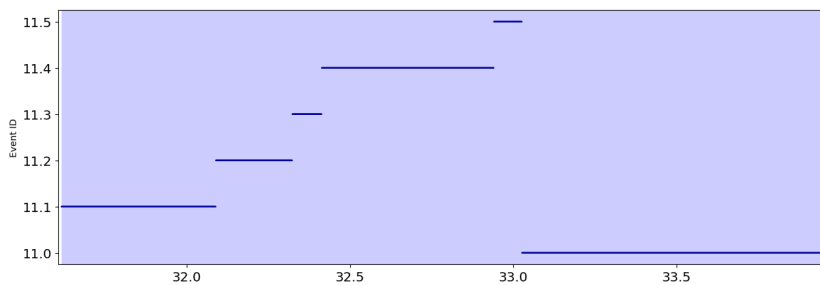


Figure 1.4: A single cleaning process and the process labels assigned during the duration. This blue rectangle corresponds to a single blue vertical line in Figure 1.5.

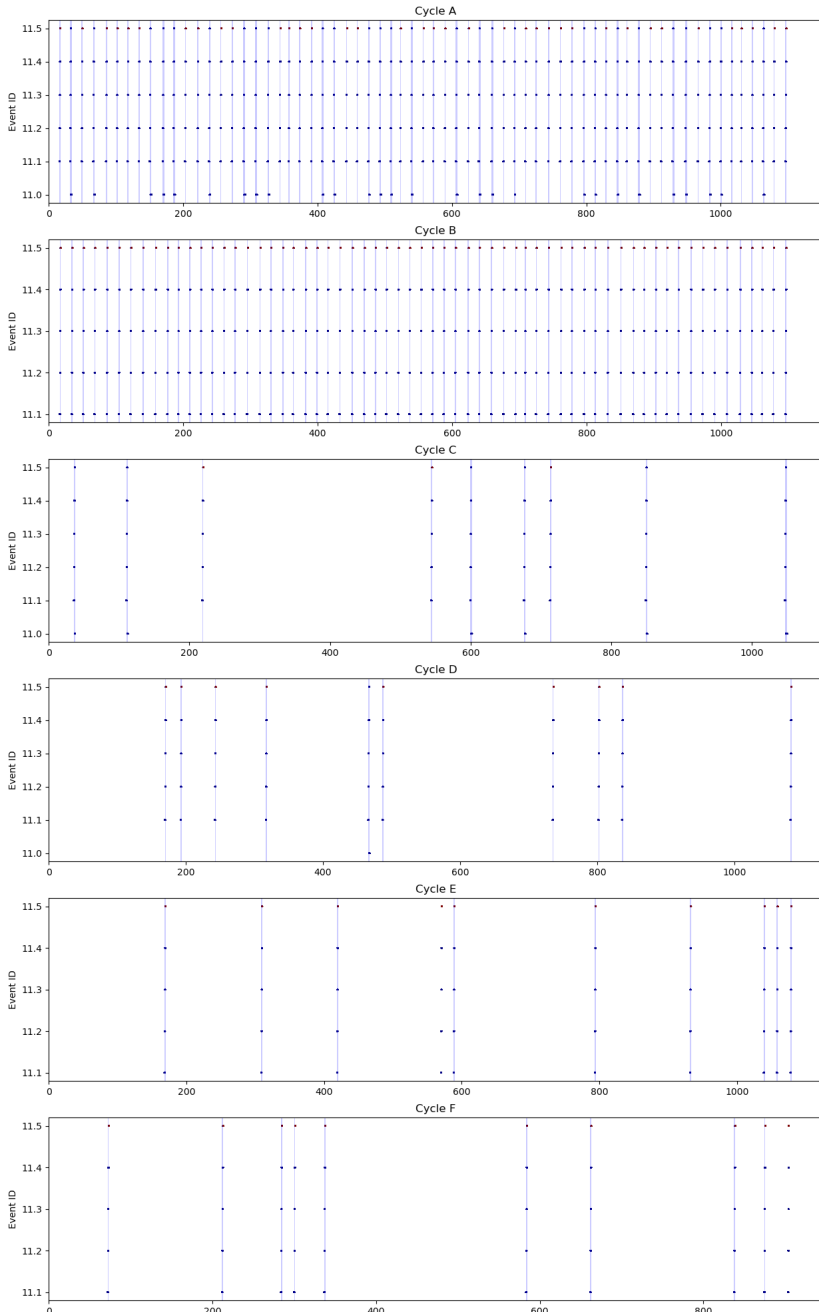


Figure 1.5: Each of the 6 cycles, cleaning (corresponding to $\text{BatchID} = 0$ in the time series dataset). Each (Cleaning process), CIP, is highlighted by an opaque interval (the blue rectangles). The dots marked with red (only process label 11.5, but not all of these are red), is if the Cleaning ID is 0 in the data. Upon further inspection, this is assumed to be the existence of delays after a cleaning process, before the next batch is started.

1.4 Suicide data

1	25	40	83	123	256
1	27	49	84	126	257
1	27	49	84	129	311
5	30	54	84	134	314
7	30	56	90	144	322
8	31	56	91	147	369
8	31	62	92	153	415
13	32	63	93	163	573
14	34	65	93	167	609
14	35	65	103	175	640
17	36	67	103	228	737
18	37	75	111	231	
21	38	76	112	235	
21	39	79	119	242	
22	39	82	122	256	

Table 1.1: The length of treatment of control patients in suicide study. The data originates from the Mental Health Enquiry (MHE) of England of Wales and was published in 1967.

1.4.1 A better spline

In theory, we could make a set of splines ourselves, that has both of the desired properties of B-splines and M-splines. I.e. a set of piecewise polynomials, which we shall denote $Q_{i,p}$, that has both the property that

$$\sum_{i=1}^n Q_{i,p}(t) = 1$$

and

$$\int_0^1 Q_{i,p}(t) dt = \frac{1}{n}$$

Actually, both M- and B-splines satisfies this for $p = 0$ as they are then both piecewise constant and non-zero on disjoint intervals. From this, one can construct such sets of $Q_{i,p}$ in the following way. Namely, start with the piecewise constant functions, $Q_{i,0}$ depicted in Figure 1.6 as boxes in the case $n = 5$.

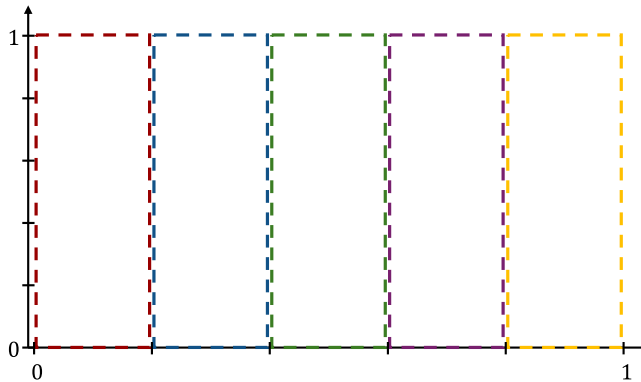


Figure 1.6: The initial splines from which we iteratively construct a set of splines summing to 1 and integrating to $1/n$ individually.

By cutting off equal areas of each of these rectangles, and moving them to the neighboring intervals as shown in Figure 1.7, we can obtain a set of splines as shown in Figure 1.8(a). In Figure 1.8(b) and Figure 1.9 we show the accumulated probability mass in each bin and the sum of the splines for all t and confirm that indeed the above properties hold. This process can be iterated to obtain more regularization/smoothing of the observations.

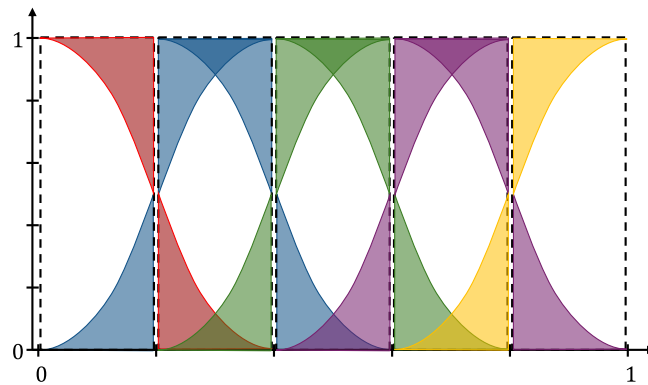


Figure 1.7: Each color represent an area removed from a rectangle and added to a neighboring interval such that the initial splines now are defined on multiple intervals, conserving the desired properties

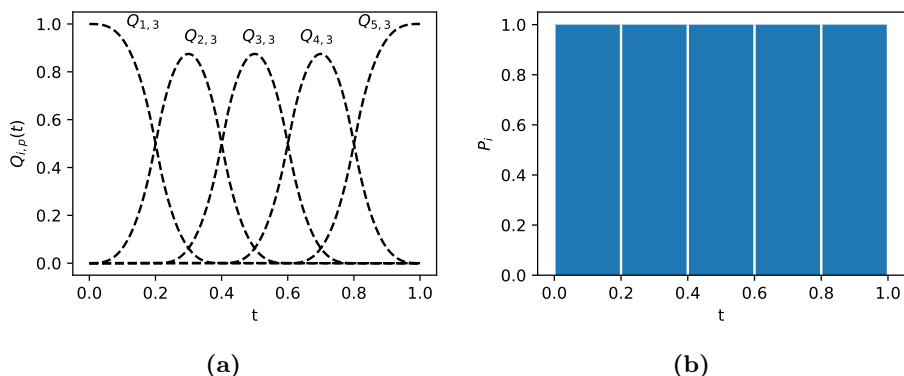


Figure 1.8: The resulting Q -splines (a) and the expected bin probability mass P_i is area of each rectangle i.e. 0.2.

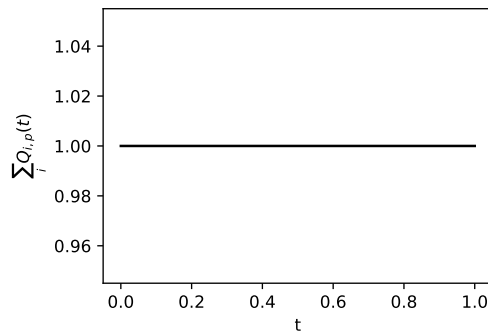


Figure 1.9: The sum of the set of Q -splines for all $t \in [0, 1]$. Indeed, they sum to 1 as per construction.

1.5 M-spline based MI estimation

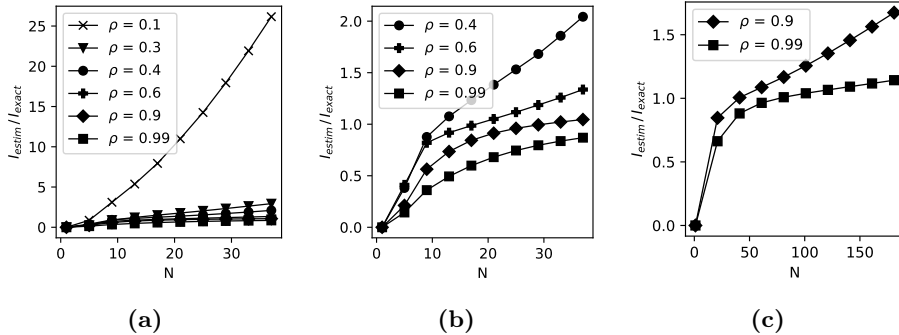


Figure 1.10: Relative errors of the mutual information using M -splines. We observe the same behavior as with the B-splines. This indicates that neither is better than the other and thus no preference between the two.

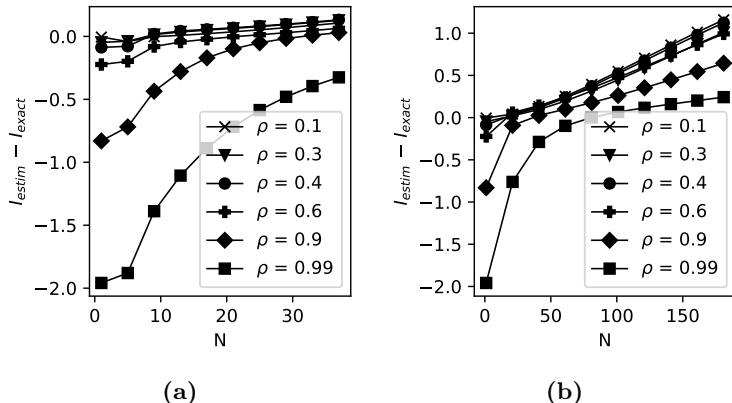


Figure 1.11: The actual error using the M-splines. Once again, we observe similar behavior to the B-splines.

1.6 Confidence interval for absolute correlation in bivariate Gaussian

From [?], given a bivariate Gaussian, the confidence distribution of ρ given the empirical correlation r based on n observations is given by

$$f(\rho | r, \nu) = \frac{\nu(\nu - 1)\Gamma(\nu - 1)}{\sqrt{2\pi}\Gamma(\nu + \frac{1}{2})} \frac{(1 - r^2)^{\frac{\nu-1}{2}} (1 - \rho^2)^{\frac{\nu-2}{2}}}{(1 - r\rho)^{\frac{2\nu-1}{2}}} F\left(\frac{3}{2}, -\frac{1}{2}, \nu + \frac{1}{2}, \frac{1 + r\rho}{2}\right)$$

where $F(a, b, c, z)$ is the Gaussian hypergeometric function and $\nu = n - 1$. That is, given a sample correlation r , what is the confidence in ρ in terms of a distribution. In the following figure, a sample correlation $r = 0.8$ and $r = 0$ has been used with varying number of observations (degrees of freedom) in figures Figure 1.12(a) and Figure 1.12(b) respectively. A key property is that f is *even*

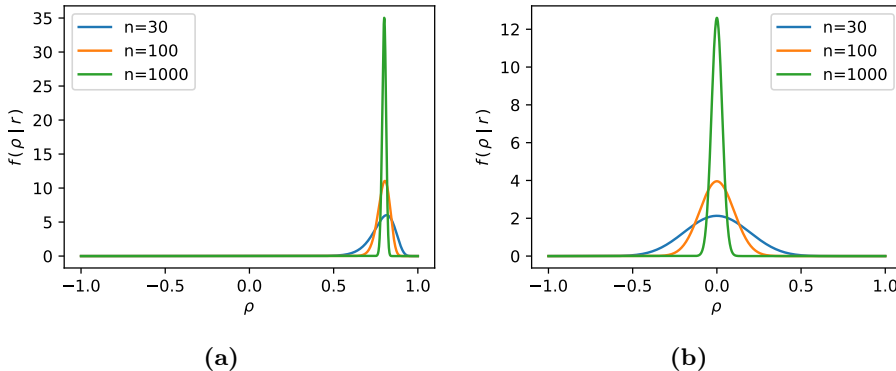


Figure 1.12: $f(\rho | r, \nu)$ shown for $r = 0.8$ and $r = 0$ in (a) and (b) with $n \in \{30, 100, 1000\}$. As one would expect, the power i.e. the width of the peak decreases with increasing n and for correlations closer to 0, the width is the largest.

symmetric in ρ, r . That is $f(\rho | r) = f(-\rho | -r)$. Thus, a confidence interval for ρ given r is the negative of the confidence interval given $-r$. In particular, if we only observe $|r|$, we can calculate a confidence interval for ρ up to the sign of the bounds of the interval. Furthermore, as we want a CI for $|\rho|$, it does not matter if r is negative or positive. Hence, without loss of generality, we assume that $r \geq 0$. At this point, to construct a confidence interval for $|\rho|$ we list the following desired properties. Firstly, it should be an exact confidence interval, meaning that for a given significance level α , the CI includes the true value exactly $1 - \alpha$ fraction of the times. Secondly, if for a given r , it can not be rejected that ρ is 0, 0 should also be contained in the interval. Finally, if we reject

that $\rho = 0$, we shall have $\alpha/2$ probability mass above and below the bounds of the interval. The above is enough to uniquely define a confidence interval in all cases. Before continuing with how this CI is calculated, we mention that as r is an unbiased estimator of ρ , we would preferably want $|r| \in CI_{1-\alpha}(|\rho|)$ (where $CI_{1-\alpha}(|\rho|)$ denotes the $1 - \alpha$ confidence interval for $|\rho|$). However, although this will in almost every scenario be the case, we can not be sure of this from the above properties and in fact examples with large α can be constructed such that $|r|$ lies just outside the constructed CI.

First, to conform with the second desired property, if it can not be rejected that $\rho = 0$ on a significance level α , we will initially compute a CI for ρ (not $|\rho|$) based on r (WLOG chosen to be non-negative). This CI will just be a symmetric CI in the sense that $\alpha/2$ of the probability mass will lie below the lower bound of the CI and above the upper bound of the CI respectively. If 0 is contained in this CI, we can not reject that $\rho = 0$ and vice versa on an α significance level. Thus, if 0 is contained in this initial CI for ρ , we will start the CI for $|\rho|$ at 0 and determine and upper bound b such that α probability mass is above this b . Otherwise, we shall find a and b such that $\alpha/2$ probability mass is below a and above b respectively. Choosing a and b this way also conforms with the third property. Finally, to ensure that the CI contains exactly $1 - \alpha$, we define \tilde{f} as the reflected f in ρ such that

$$\tilde{f}(\rho_a | r_a, \nu) = f(\rho_a | r_a, \nu) + f(-\rho_a | r_a, \nu), \quad \rho_a, r \in [0, 1]$$

where ρ_a and r_a is the absolute correlation and empirical correlation respectively. With this \tilde{f} , the density at ρ_a is both the density for the negative and positive correlation ensuring that the \tilde{f} has probability mass 1. Thus, if $a = 0$ (i.e. the CI must contain 0), we find b as the $1 - \alpha$ percentile of \tilde{f} and if $a \neq 0$, we take a as the $\alpha/2$ percentile and b as the $1 - \alpha/2$ percentile of \tilde{f} .

As an example, suppose $r_a = 0.06$ with 1000 observations. Then a 95% CI for $|\rho|$ is $[0, 0.11164]$ whereas if one had observed $r_a = 0.07$ the CI would be $[0.01071, 0.1314]$. These CI could then be used to test the absolute correlation of a bivariate Gaussian i.e. for $r_a = 0.07$ based on 1000 observations would be rejected as stemming from a Gaussian with absolute correlation 0.01 on a 5% significance level.

1.7 Gaussian chain deconvolution

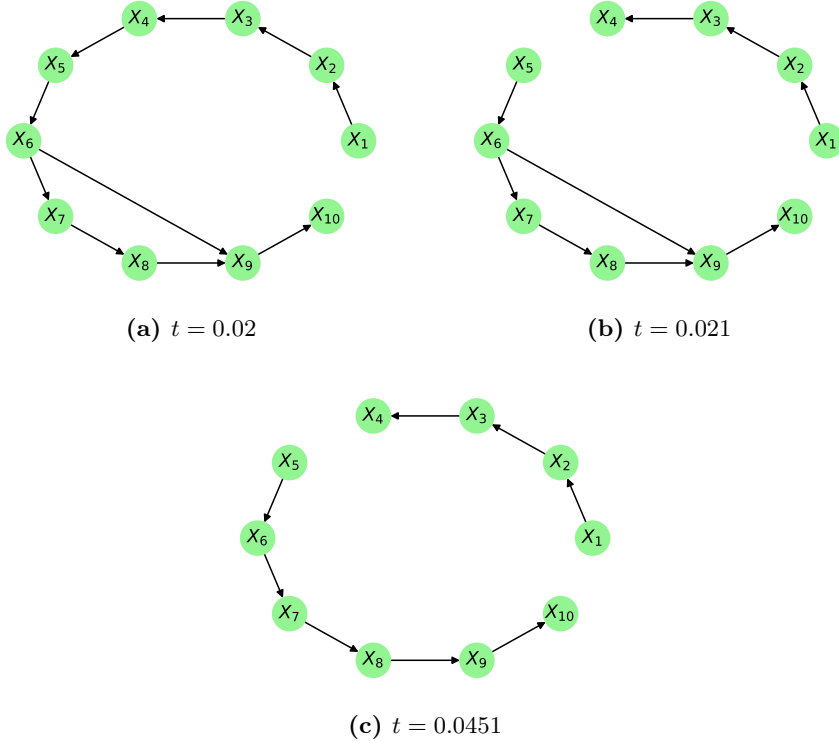


Figure 1.13: G_{dir} represented as a graph for different cut-offs. Based on a triangular G_{obs} with mutual information as the measure of similarity. Varying the threshold, we observe that we are almost able to recover the true causal structure. Only the weak link between variables X_4 and X_5 .

1.8 Gaussian network deconvolution

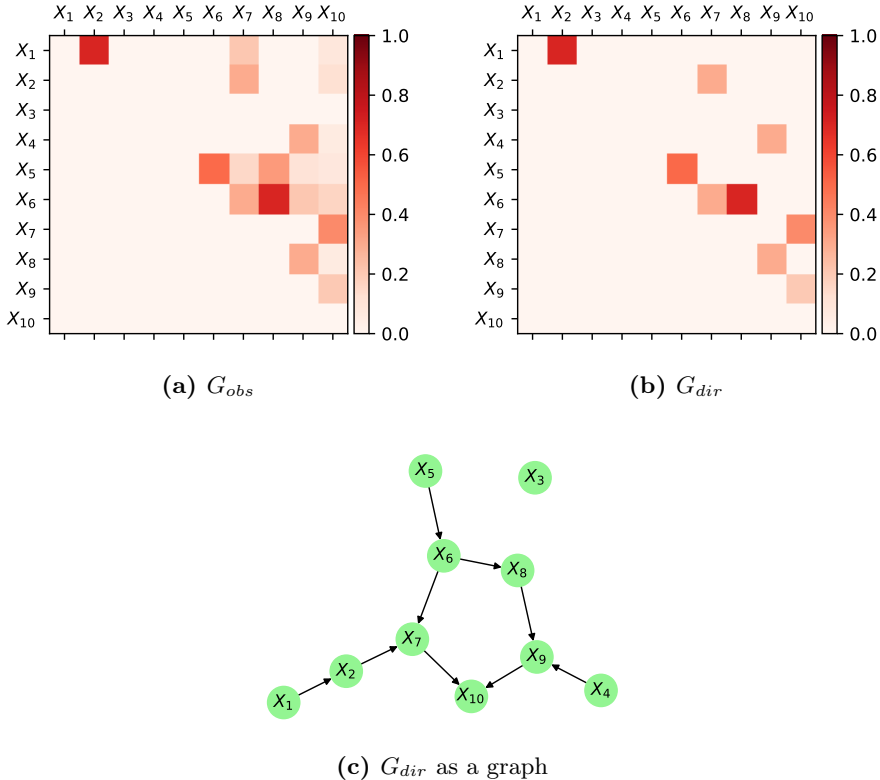


Figure 1.14: For the linear network defined in ??, using a triangular G_{obs} (a) with the true topological structure and correlation as the measure of similarity we are able to perfectly rediscover the causal structure as seen in (b) and (c).

1.9 Pharmaceutical process deconvolution

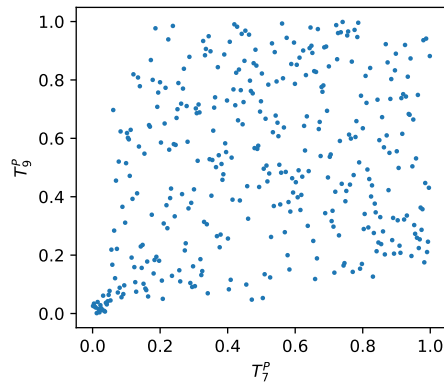


Figure 1.15: T_9^P vs T_7^P for the pharmaceutical data set. Although a small positive correlation is observed, it does not appear as if these variables are particularly descriptive of each other.

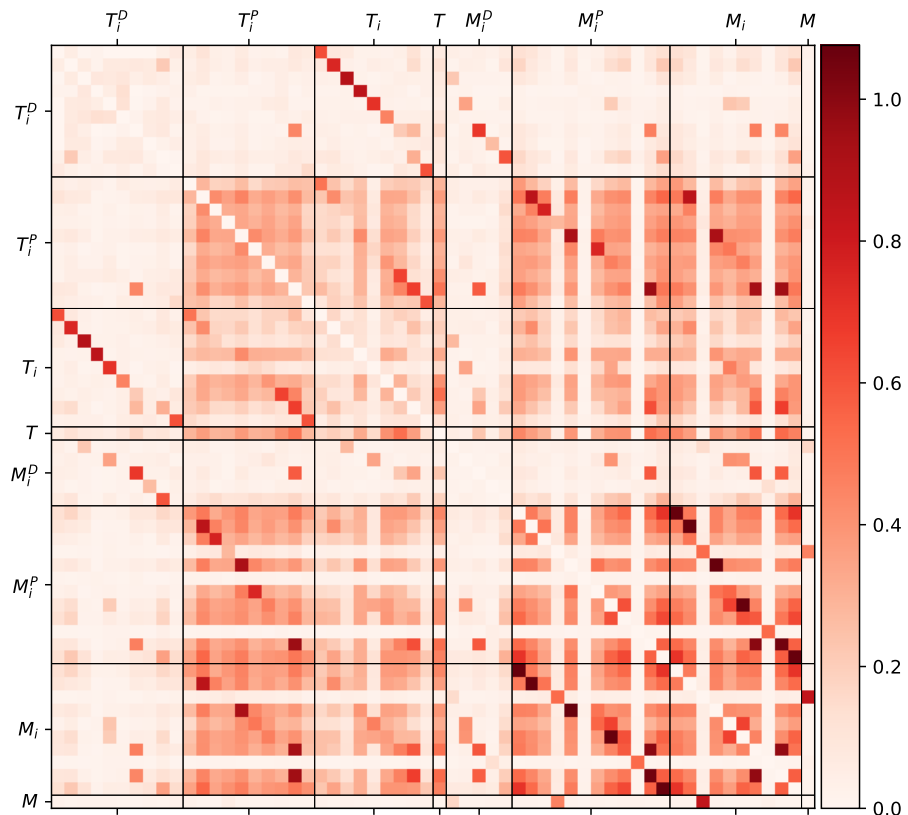


Figure 1.16: G_{obs} from pharmaceutical production data. Strong dependencies between variables and the related accumulated variables are observed.

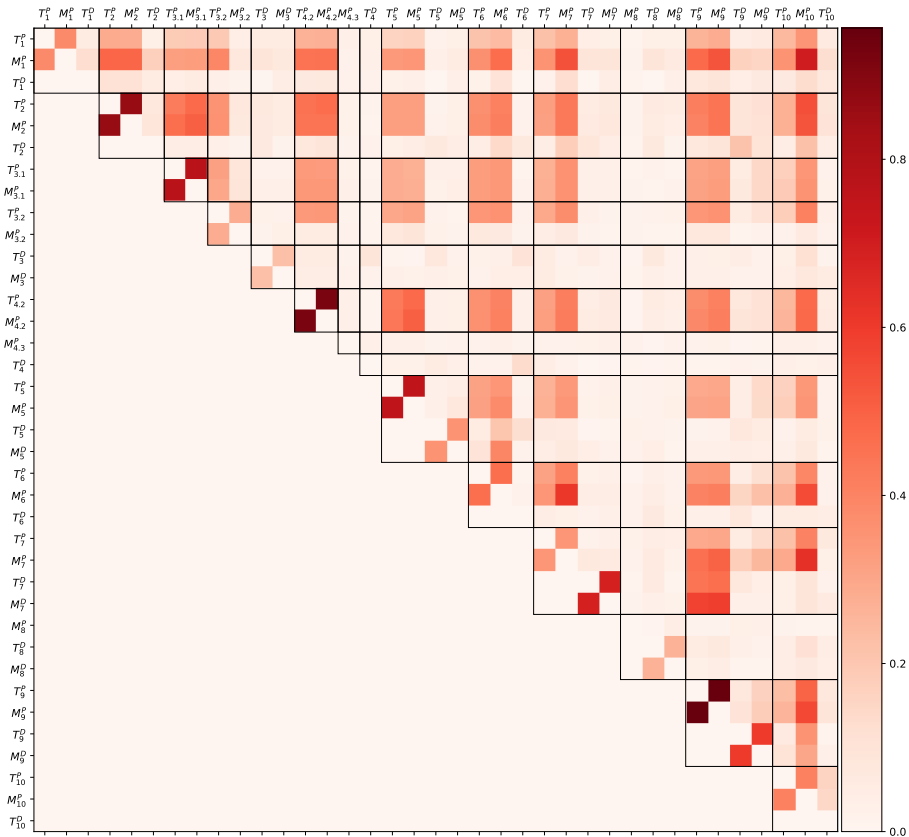


Figure 1.17: G_{obs} for both durations, delays and level changes for the simulated data from [?]. Labels related to the same process are divided by lines vertically and horizontally to easier observe what is related to what.